CHINESE OPTICS LETTERS

Vol. 20, No. 4 | April 2022

Highly integrated photonic crystal bandedge lasers monolithically grown on Si substrates

Yaoran Huang (黄要然)[1,†], Taojie Zhou (周陶杰)[1,2,†], Mingchu Tang (唐明初)[2], Guohong Xiang (项国洪)[1], Haochuan Li (李浩川)[1], Mickael Martin[3], Thierry Baron[3], Siming Chen (陈思铭)[2], Huiyun Liu (刘会赟)[2], and Zhaoyu Zhang (张昭宇)[1*]

[1] School of Science and Engineering and Shenzhen Key Laboratory of Semiconductor Lasers, The Chinese University of Hong Kong, Shenzhen (CUHKSZ), Shenzhen 518172, China

[2] Department of Electronic and Electrical Engineering, University College London, London WC1E 7JE, UK

[3] Université Grenoble Alpes, CNRS, CEA-LETI, MINATEC, LTM, F-38054 Grenoble, France

*Corresponding author: zhangzy@cuhk.edu.cn

Received November 16, 2021 | Accepted January 14, 2022 | Posted Online February 16, 2022

Monolithic integration of III-V lasers with small footprint, good coherence, and low power consumption based on a CMOS-compatible Si substrate have been known as an efficient route towards high-density optical interconnects in the photonic integrated circuits. However, the material dissimilarities between Si and III-V materials limit the performance of monolithic microlasers. Here, under the pumping condition of a continuous-wave 632.8 nm He–Ne gas laser at room temperature, we achieved an InAs/GaAs quantum dot photonic crystal bandedge laser, which is directly grown on an on-axis Si (001) substrate, which provides a feasible route towards a low-cost and large-scale integration method for light sources on the Si platform.

Keywords: lasers; bandedge; photonic crystal; monolithic integration; quantum dots; silicon substrate.

DOI: 10.3788/COL202220.041401

1. Introduction

Advanced microscale silicon photonics technology has emerged as a promising candidate for the next-generation chip-scale data communication network due to its unique advantages of low cost, high integration density, high speed, and energy efficiency[1,2]. However, a highly efficient microscale Si-based light source is still considered as the obstacle for realizing a practical Si-based photonic integrated circuit (PIC), due to the indirect bandgap nature of bulk Si and Ge materials.Various approaches towards integration of microcavity lasers on silicon substrates have been demonstrated extensively, including co-packing, hybrid integration, wafer bonding, etc. But, these methods more or less include cumbersome fabrication processes[1,2]. The monolithic integration method, however, is another promising route towards low cost and scalable Si-based PICs. Monolithic integration takes advantage of the CMOS-compatible fabrication process of contemporary integrated circuits. It is unnecessary to consider heterogenous methods to make precise alignment between the light souce and other optical components. Nevertheless, the fundamental challenge of epitaxial III-V on Si is the degraded material quality caused by large material dissimilarities[3]. The planar defect and anti-phase boundary, due to the polar on non-polar growth, can be avoided by employing a pretreated double-atomic-step Si substrate[4]. Furthermore, a strained-layer superlattice (SLS) has been used as defect filter layers (DFLs) to significantly reduce the threading defect caused by the lattice mismatched heteroepitaxial growth of III–V materials on Si[5]. Those works pave the way for high-performance ridge-waveguide lasers with quantum dot (QD) gain medium directly grown on the group-IV substrates through various intermediate buffer layers and offcut substrates, including Ge[6], Ge-on-Si[7], GaP/Si(001)[8], patterned on-axis Si (001)[9], and Si substrate with a 4° offcut angle[3]. However, the relatively large footprint of the ridge-waveguide laser limits the realization of microscale Si-based PICs. Recently, we have demonstrated InAs/GaAs QD microdisk lasers and photonic crystal membrane lasers monolithically grown on CMOS-compatible on-axis Si (001) substrates[10–12].

Meanwhile, defect-free photonic crystal bandedge laser arrays enable a large-area coherent oscillation, so a large number of attractive applications have been derived[13,14], including laser-based processing and light detection. The group velocity of high symmetry points in the energy band diagram can be very low. When a mode with group velocity is close to zero in the material gain region, the bandedge effect occurs. There is a large increase in optical path length for the bandedge point, which significantly improves the effective gain. Various

© 2022 Chinese Optics Letters

high-performance photonic crystal bandedge surface emitting lasers have been demonstrated with high output power and single mode emission[15,16].

In this paper, we demonstrate InAs/GaAs QD square lattice photonic crystal bandedge lasers monolithically grown on an on-axis Si (001) substrate with ultra-low lasing threshold under 632.8 nm He–Ne gas laser source at room temperature. This square lattice photonic crystal bandedge laser on Si can be a promising candidate for the coherent light source for Si photonics due to its low threshold characteristic and potential capability for high-power output.

2. Device Fabrication

The doping-free CMOS-compatible on-axis Si (001) substrates are offered for the monolithic growth of InAs/GaAs QD photonic crystal bandedge lasers[11,12]. The as-grown 400 nm GaAs layer is on the on-axis Si (001) substrate with a 0.15° misorientation with two steps by metalorganic chemical vapor deposition, and then the substrate is transferred to the molecular beam epitaxy (MBE) chamber for subsequent material growth. Four sets of optimized DFLs are grown after a 200 nm of GaAs buffer layer, which is grown at 580°C to make the epitaxial surface smooth, while each set of DFLs contains a low-temperature growth of $In_{0.18}Ga_{0.82}As/GaAs$ SLSs at 450°C, followed by an *in-situ* thermal annealing at 600°C for 5 min, and then a 300 nm GaAs spacer layer is covered at the top with high temperature. Figure 1(a) shows the specific details of the epitaxial structure of the active layer, and four-stack as-grown InAs/InGaAs dot-in-well (DWELL) active layers used as the gain materials were grown on a 1 μm $Al_{0.6}Ga_{0.4}As$ sacrificial layer[11,12,17], which were sandwiched by two symmetrical 40 nm $Al_{0.4}Ga_{0.6}As$ cladding layers. Each stack of DWELL layers consists of 2.7 monolayer InAs QDs grown at 510°C on a 2 nm $In_{0.15}Ga_{0.85}As$ layer and capped by a 6 nm $In_{0.15}Ga_{0.85}As$ layer, followed by a 5 nm low-temperature grown GaAs layer and 45 nm high-temperature grown GaAs spacer layer at 600°C. Figure 1(b) illustrates a high-resolution transmission electron microscope (TEM) image of a single QD, with a typical size of 25 nm in diameter. Figure 1(c) presents uncapped InAs/GaAs QDs grown on the Si (001) substrate, which is captured by an atomic force microscope (AFM) with a density of about $4 \times 10^{10}\ cm^{-2}$. The optical property of as-grown QDs is investigated by a micro-photoluminescent (μ-PL) measurement under room temperature, as presented in Fig. 1(d), showing various PL spectra under different continuous-wave optically pumping powers from 1 μW to 420 μW. A ground state emission of 1322 nm is observed, accompanying a first excited state of 1240 nm. PL emission from the further excited states of QDs is pumped out while increasing the powers. Furthermore, an integrated PL intensity driven from temperature dependent PL measurement is presented in the inset of Fig. 1(d), showing a thermal activation energy of approximately 270 meV, which is fitted by the Arrhenius equation.

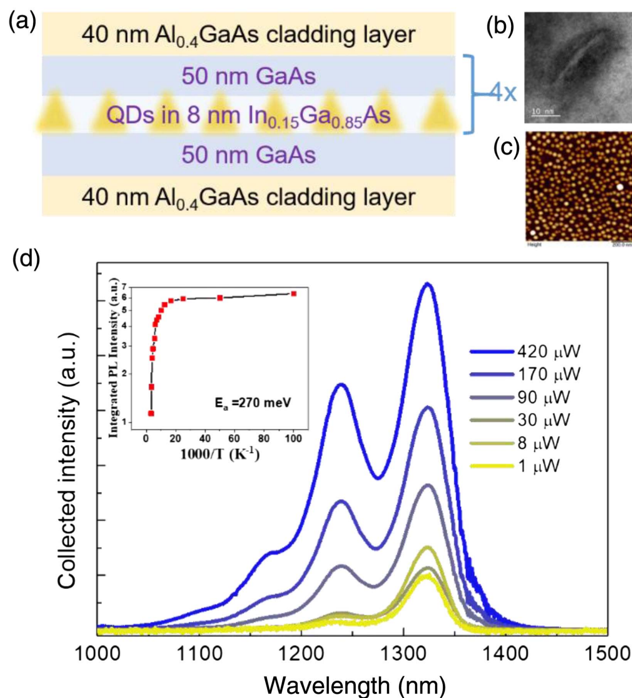

Fig. 1. (a) Schematic epitaxial structure of the active region with total thickness of ~ 362 nm. (b) A high-resolution TEM image of a single InAs QD. (c) An AFM image of uncapped InAs/GaAs QDs. (d) Collected PL spectra of the as-grown structure under various input optical powers at room temperature. Inset: temperature dependent integrated PL intensity.

Figure 2(a) shows the schematic figure of the photonic crystal bandedge lasers monolithically grown on an on-axis Si (001) substrate, and the lattice constant *a* and the air holes diameter 2*r* are pointed in the inset. The suspended structure is formed by wet etching the sacrificial layer underneath the active layer due to the different etching selection ratios. The purpose of the suspended structure is to better confine the light in the vertical direction, where the active layer is sandwiched by air.

The fabrication processes of this bandedge laser are presented with these steps. First, plasma-enhanced chemical vapor deposition (PECVD) was used for depositing ~120 nm SiO_2 as a hard mask. Then, 160 nm Zep520 e-beam resist was spin-coated on the surface, and the pattern of the photonic crystal bandedge cavities array was defined by using electron-beam lithography

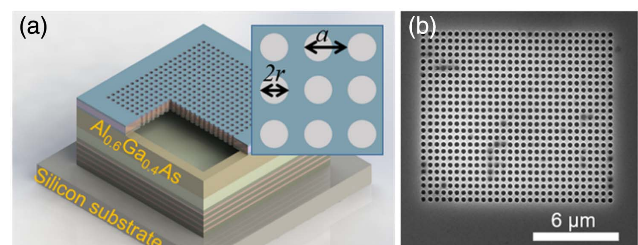

Fig. 2. (a) Schematic diagram of the fabricated InAs/GaAs QD bandedge laser directly grown on an on-axis Si (001) substrate. The lattice constant and radius of air holes are *a* and *r*, respectively. (b) An SEM image of fabricated photonic crystal bandedge cavity.

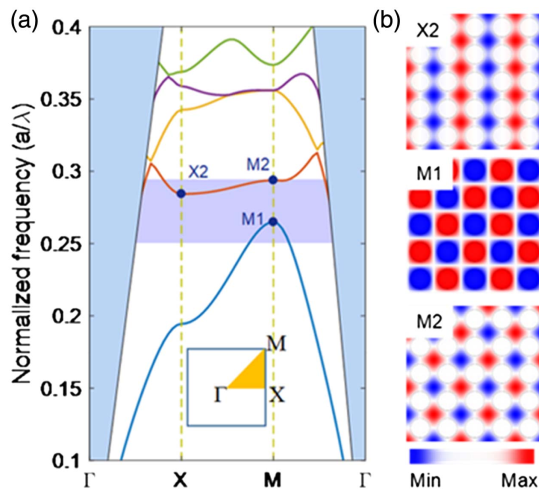

Fig. 3. (a) Dispersion relation diagram of TE-like states for the photonic crystal bandedge cavity with the parameters of $r/a = 0.35$ and the slab thickness of $1.05a$. The inset shows the irreducible Brillouin zone. The shaded blue region indicates the light cone, and the purple area represents the gain region of as-grown QDs. High symmetry points with low group velocity within the gain region are marked as X2, M1, and M2. (b) The corresponding calculated hertz (Hz) field profiles.

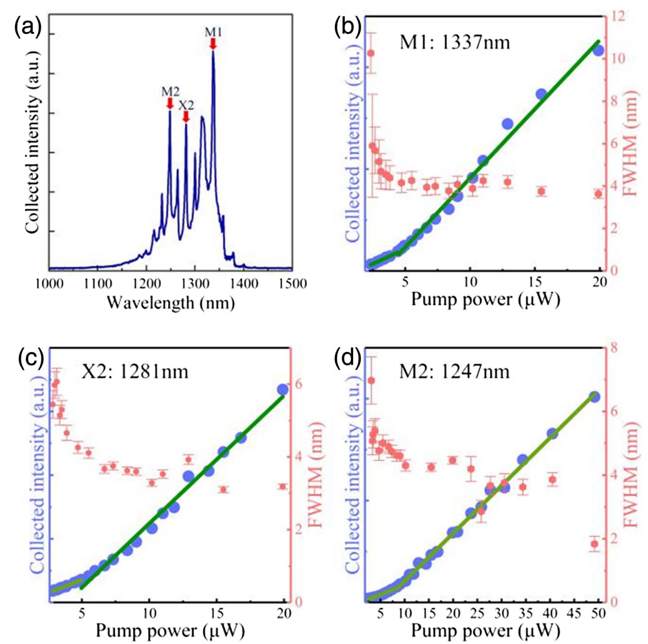

Fig. 4. (a) Emission spectrum of the fabricated photonic crystal bandedge laser, the pump power is 49.2 μW. Lasing modes of M1, X2, and M2 can be determined by the spectral positions. (b)–(d) The L-L curve and FWHM as a function of input power for three lasing modes M1, X2, and M2, respectively.

(EBL) and followed by development. The hard mask is etched by inductively coupled plasma (ICP) reactive ion etching to transfer the pattern. After the removal of the remaining resist, ICP is used for further transformation of the square lattice photonic crystal array to the active region. The wet-etching process was implemented to remove the hard mask and to undercut the sacrificial layer for the formation of a free-standing photonic crystal structure. The fabricated photonic crystal bandedge cavity is shown in Fig. 2(b), which is captured by a scanning electron microscope (SEM).

3. Discussion

The dispersion relation diagram and the corresponding eigenfield profiles were calculated by MIT photonic bands (MPBs) based on the plane-wave expansion method[18]. The dispersion relation diagram of TE-like states is illustrated in Fig. 3(a), with the bandedge cavity parameters of lattice constant $a = 340$ nm, $r/a = 0.35$, and the slab thickness $\sim 1.05a$. The light cone is indicated by the blue region. The approximate optical gain region (from 1194 nm to 1340 nm) of the as-grown QDs was represented by the purple region, covering both the ground state and the first excited state obtained by curve fitting of the collected PL spectra. Three bandedge modes at high symmetry points M1, X2, and M2 are possible for the lasing emission because of their locations in the gain region. The corresponding magnetic field profiles of X2, M1, and M2 are depicted in Fig. 3(b). For further research, to realize single mode emission, some methods can be implemented such as by slightly modifying the parameters of the photonic crystal bandedge cavity to enable only one bandedge point lying within the as-grown InAs QDs gain region for single mode lasing. Introducing the taper region (with linear decrease of air holes) at the Γ point to reduce radiation loss at X2 can also be a convincing way.

A μ-PL system setup was used to characterize the fabricated photonic crystal bandedge lasers. We optically pumped the bandedge cavity at room temperature with a standard 632.8 nm He–Ne gas laser as the pumping source, whose standard Gaussian spot size is around 3 μm. The PL spectrum of this cavity with $a = 340$ nm and $r/a = 0.35$ is shown in Fig. 4(a). M2, X2, and M1 points with low group velocity are shown in Fig. 4(a), and the spectral positions of lasing modes are comparable with the calculated normalized frequencies. The light-out light-in (L-L) curves of the three modes are shown in Figs. 4(b)–4(d), with a linewidth narrowing observed. But, it is worth mentioning that due to some imperfection fabrication results, the full width at half maximum (FWHM) ~3 nm lasing modes are relatively large. The optimization of etching can make the surface of the photonic crystal bandedge cavity smoother, the sidewall of the air holes more vertical, and the diameter of the air holes close to the simulation result, so as to solve the problem of large FWHM. The bandedge modes M1 and X2 emissions peaking at 1337 nm and 1281 nm are within the ground state with a lasing threshold around 4 μW and 5 μW, respectively, while the bandedge mode M2 with a peak wavelength of 1247 nm was in the first excited state, of which the threshold is ~7.5 μW.

4. Conclusion

In conclusion, we have demonstrated InAs/GaAs QD square lattice photonic crystal bandedge lasers monolithically grown on

on-axis Si (001) substrates. The lasers operated under continuous-wave optical pumping at room temperature. An ultra-low lasing threshold was observed in a multi-mode lasing operation. With further structure design or optimized plasma-etching profiles, a single mode lasing emission is feasible. The demonstrated photonic crystal bandedge lasers monolithically grown on the Si substrate are a promising candidate as a large-scale coherent light source for Si photonics.

Acknowledgement

This research was supported by the National Natural Science Foundation of China (No. 62174144), Shenzhen Fundamental Research Fund (Nos. JCYJ20210324115605016 and JCYJ20210324120204011), Optical Communication Core Chip Research Platform, Shenzhen Key Laboratory Project (No. ZDSYS201603311644527), Longgang Key Laboratory Project (Nos. ZSYS2017003 and LGKCZSYS2018000015), Longgang Matching Support Fund (Nos. CXPTPT-2017-YJ-002 and 201617486), President's Fund (PF01000154), UK Engineering and Physical Sciences Research Council (EP/P006973/1 and National Epitaxy Facility), European project H2020-ICT-PICTURE (780930), Royal Academy of Engineering (RF201617/16/28), and French government managed by ANR under the Investissements davenir ANR-10-IRT-05 and ANR-15-IDEX-02 and French RENATECH network.

The devices were manufactured in Core Research Facilities (CRF) at SUSTech, and the authors thank the engineers for their technical support.

[†]These authors contributed equally to this work.

References

1. D. Thomson, A. Zilkie, J. E. Bowers, T. Komljenovic, G. T. Reed, L. Vivien, D. Marris-Morini, E. Cassan, L. Virot, J.-M. Fédéli, J.-M. Hartmann, J. H. Schmid, D.-X. Xu, F. Boeuf, P. O'Brien, G. Z. Mashanovich, and M. Nedeljkovic, "Roadmap on silicon photonics," J. Opt. **18**, 073003 (2016).
2. M. Asghari and A. V. Krishnamoorthy, "Energy-efficient communication," Nat. Photonics **5**, 268 (2011).
3. S. Chen, W. Li, J. Wu, Q. Jiang, M. Tang, S. Shutts, S. N. Elliott, A. Sobiesierski, A. J. Seeds, I. Ross, P. M. Smowton, and H. Liu, "Electrically pumped continuous-wave III-V quantum dot lasers on silicon," Nat. Photonics **10**, 307 (2016).
4. R. Alcotte, M. Martin, J. Moeyaert, R. Cipro, S. David, F. Bassani, F. Ducroquet, Y. Bogumilowicz, E. Sanchez, Z. Ye, X. Y. Bao, J. B. Pin, and T. Baron, "Epitaxial growth of antiphase boundary free GaAs layer on 300 mm Si (001) substrate by metalorganic chemical vapour deposition with high mobility," APL Mater. **4**, 046101 (2016).
5. M. Tang, S. Chen, J. Wu, Q. Jiang, K. Kennedy, P. Jurczak, M. Liao, R. Beanland, A. Seeds, and H. Liu, "Optimizations of defect filter layers for 1.3-μm InAs/GaAs quantum-dot lasers monolithically grown on Si substrates," IEEE J. Sel. Top. Quantum Electron. **22**, 50 (2016).
6. H. Liu, T. Wang, Q. Jiang, R. Hogg, F. Tutu, F. Pozzi, and A. Seeds, "Long-wavelength InAs/GaAs quantum-dot laser diode monolithically grown on Ge substrate," Nat. Photonics **5**, 416 (2011).
7. A. Lee, Q. Jiang, M. Tang, A. Seeds, and H. Liu, "Continuous-wave InAs/GaAs quantum-dot laser diodes monolithically grown on Si substrate with low threshold current densities," Opt. Express **20**, 22181 (2012).
8. D. Jung, J. Norman, M. Kennedy, C. Shang, B. Shin, Y. Wan, A. C. Gossard, and J. E. Bowers, "High efficiency low threshold current 1.3 μm InAs quantum dot lasers on on-axis (001) GaP/Si," Appl. Phys. Lett. **111**, 122107 (2017).
9. Y. Wan, Q. Li, A. Y. Liu, A. C. Gossard, J. E. Bowers, E. L. Hu, and K. M. Lau, "Optically pumped 1.3 μm room-temperature InAs quantum-dot micro-disk lasers directly grown on (001) silicon," Opt. Lett. **41**, 1664 (2016).
10. T. Zhou, M. Tang, G. Xiang, B. Xiang, S. Hark, M. Martin, M.-L. Touraton, T. Baron, Y. Lu, S. Chen, H. Liu, and Z. Zhang, "Ultra-low threshold InAs/GaAs quantum dot microdisk lasers on planar on-axis Si (001) substrates," Optica **11**, 430 (2020).
11. T. Zhou, M. Tang, G. Xiang, X. Fang, X. Liu, B. Xiang, S. Hark, M. Martin, T. Baron, S. Pan, J.-S. Park, Z. Liu, S. Chen, Z. Zhang, and H. Liu, "Continuous-wave quantum dot photonic crystal lasers grown on on-axis Si (001)," Nat. Commun. **11**, 977 (2020).
12. T. Zhou, M. Tang, H. Li, Z. Zhang, Y. Cui, J.-S. Park, M. Martin, T. Baron, S. Chen, H. Liu, and Z. Zhang, "Single-mode photonic crystal nanobeam lasers monolithically grown on Si for dense integration," IEEE J. Sel. Top. Quantum Electron. **28**, 1501906 (2021).
13. H.-Y. Ryu, S.-H. Kwon, Y.-J. Lee, Y.-H. Lee, and J.-S. Kim, "Very-low-threshold photonic band-edge lasers from free-standing triangular photonic crystal slabs," Appl. Phys. Lett. **80**, 3476 (2002).
14. S.-H. Kwon, H.-Y. Ryu, G.-H. Kim, Y.-H. Lee, and S.-B. Kim, "Photonic bandedge lasers in two-dimensional square-lattice photonic crystal slabs," Appl. Phys. Lett. **83**, 3870 (2003).
15. H.-Y. Lu, S.-C. Tian, C.-Z. Tong, L.-J. Wang, J.-M. Rong, C.-Y. Liu, H. Wang, S.-L. Shu, and L.-J. Wang, "Extracting more light for vertical emission: high power continuous wave operation of 1.3-μm quantum-dot photonic-crystal surface-emitting laser based on a flat band," Light Sci. Appl. **8**, 108 (2019).
16. S. Noda, K. Kitamura, T. Okino, D. Yasuda, and Y. Tanaka, "Photonic-crystal surface-emitting lasers: review and introduction of modulated-photonic crystals," IEEE J. Sel. Top. Quantum Electron. **23**, 4900107 (2017).
17. H. Y. Liu, I. R. Sellers, T. J. Badcock, D. J. Mowbray, M. S. Skolnick, K. M. Groom, M. Gutierrez, M. Hopkinson, J. S. Ng, J. P. R. David, and R. Beanland, "Improved performance of 1.3 μm multilayer InAs quantum-dot lasers using a high-growth-temperature GaAs spacer layer," Appl. Phys. Lett. **85**, 704 (2004).
18. S. G. Johnson and J. D. Joannopoulos, "Block-iterative frequency-domain methods for Maxwell's equations in a planewave basis," Opt. Express **8**, 173 (2001).